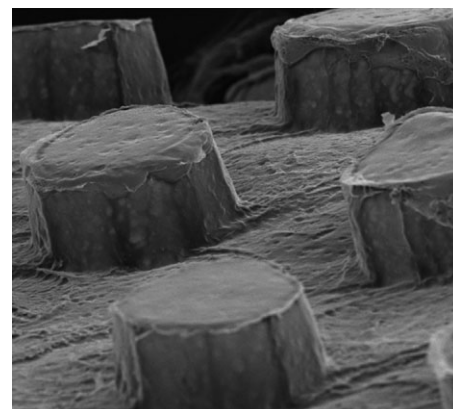


# Construction of a Microstructured Collagen Membrane Mimicking the Papillary Dermis Architecture and Guiding Keratinocyte Morphology and Gene Expression

Gerwen Lammers, Günter Roth, Mathias Heck, Roland Zengerle, G. Sandra Tjabringa, Elly M. Versteeg, Theo Hafmans, Ronnie Wismans, Dieter P. Reinhardt, Eugene T. P. Verwiel, Patrick L. J. M. Zeeuwen, Joost Schalkwijk, Roland Brock, Willeke F. Daamen, Toin H. van Kuppevelt\*

A papillary-structured collagen fibril membrane is created, mimicking the 3D-architecture of the human papillary dermis. Primary human keratinocytes cultured to confluency on papillar-structured films are compared to keratinocytes cultured on flat membranes. Microscopical evaluation reveals the presence of morphologically distinct cells at the base of the papillar structures that are not observed on flat membranes. Gene expression microarrays and RT-qPCR indicate that these cells are in a more proliferative/migrational state, whereas cells on flat membranes have a more differentiated expression profile. Immunohistochemical stainings confirm these results. In conclusion, specific collagen architecture can direct keratinocyte behavior, and this may be used to further improve skin regeneration.



Dr. G. Lammers, E. M. Versteeg, T. Hafmans, R. Wismans, Prof. R. Brock, Dr. W. F. Daamen, Dr., T. H. van Kuppevelt  
Department of Biochemistry 280, Nijmegen Centre for Molecular Life Sciences, Radboud University Nijmegen Medical Centre, P.O. Box 9101, 6500 HB Nijmegen, The Netherlands  
E-mail: a.vanKuppevelt@ncmls.ru.nl

Dr. G. Roth, M. Heck, Prof. R. Zengerle  
Laboratory for MEMS Applications, Department of Microsystems Engineering (IMTEK) University of Freiburg, Georges-Koehler-Allee 106, D-79110 Freiburg, Germany

Dr. G. Roth, Prof. R. Zengerle  
HSG-IMIT, Wilhelm-Schickard-Straße 10, D-78052 Villingen-Schwenningen, Germany

Dr. G. Roth, Prof. R. Zengerle  
BIOSS Centre for Biological Signalling Studies, Albert-Ludwigs-Universität Freiburg, Germany

Dr. G. S. Tjabringa, Dr. P. L. J. M. Zeeuwen, Prof. J. Schalkwijk  
Department of Dermatology 370, Nijmegen Centre for Molecular Life Sciences, Radboud University Nijmegen Medical Centre, P.O. Box 9101 6500 HB Nijmegen, The Netherlands

Dr. D. P. Reinhardt  
Department of Anatomy and Cell Biology, McGill University, Montreal, Canada

Dr. E. T. P. Verwiel  
Department of Human Genetics 855, Nijmegen Centre for Molecular Life Sciences, Radboud University Nijmegen Medical Centre, P.O. Box 9101, 6500 HB Nijmegen, The Netherlands

## 1. Introduction

Healing of large full-thickness wounds and deep burns often results in contraction and scar tissue formation.<sup>[1]</sup> To guide and improve the wound healing process, tissue-engineered skin constructs based on natural and synthetic biomaterials have been developed.<sup>[2,3]</sup> Results of treatment with these constructs are promising, but not optimal and there is still space for improvement. For example, regeneration of the characteristic rete ridge morphology of the dermal-epidermal-junction may result in better skin regeneration (Figure 1).

Rete ridges are thickenings of the epidermis that extend downwards between the dermal papillae. The papillae provide epidermal cells with oxygen and nutrients, and reinforce the attachment of the epidermis to the dermis. In addition, several studies have indicated that defined locations in rete ridges serve as potential niches for epidermal stem cells.<sup>[4,5]</sup> These locations may provide a specific microenvironment that is required for stem cell maintenance. However, the proposed relationship between rete ridge location and cellular “stemness” remains controversial.<sup>[6–8]</sup>

Microstructured biomaterials may be used to stimulate the formation of epidermal rete ridges and dermal papillae. In addition, the availability of papillary-structured membranes may facilitate fundamental research to the relationship between keratinocyte niche and function. Cells (including keratinocytes) have been evaluated on three-dimensional microstructured surfaces, including grooved membranes composed of natural collagen and glycosaminoglycans.<sup>[9,10]</sup> However, the latter study used parallel grooves, which are technically less complex to produce than more natural rounded structures. In one study, polydimethylsiloxane (PDMS) pillars were coated with fibronectin and it was found that the interspace distance determined keratin 1 expression in cultured keratinocytes.<sup>[11]</sup>

In this study, a microstructured collagen membrane was constructed and evaluated, mimicking the natural 3D-architecture of the papillary dermis of human skin.<sup>[12]</sup>

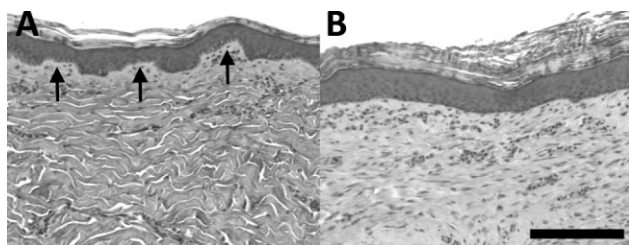


**Figure 1.** (A) The dermal-epidermal junction of normal porcine skin showing rete ridges and dermal papillae (arrows) on microscopic sections. (B) These structures are not observed in regenerated skin (in this example 55 d after treatment with a porous collagen scaffold). Bar is 100  $\mu\text{m}$ .

The *in vitro* response of primary human keratinocytes to this papillary-structured membrane was studied using high density gene expression microarrays, quantitative polymerase chain reaction (PCR), electron microscopy, and (immuno)cytochemistry. This study is unique in its use of a combination of natural materials and dimensions, and the comprehensive analysis of the biological effects.

## 2. Results

### 2.1. Construction of Microstructured Collagen Membranes Mimicking the Papillary Dermis

A polycarbonate master was constructed based on literature values for dermal papillae architecture in the human inner forearm (Figure 2).<sup>[12]</sup> The master closely matched the general architecture of the dermal papillae and could be used to produce multiple PDMS molds. One PDMS mold (Figure 3A) was used to produce multiple papillary-structured collagen membranes (Figure 3B–D). It was found essential to completely fill the pits of the mold by de-aeration of the collagen suspension before air-drying. Dry membranes could easily be peeled off and it was possible to reuse the mold multiple times without complications. The architecture of the papillary-structured

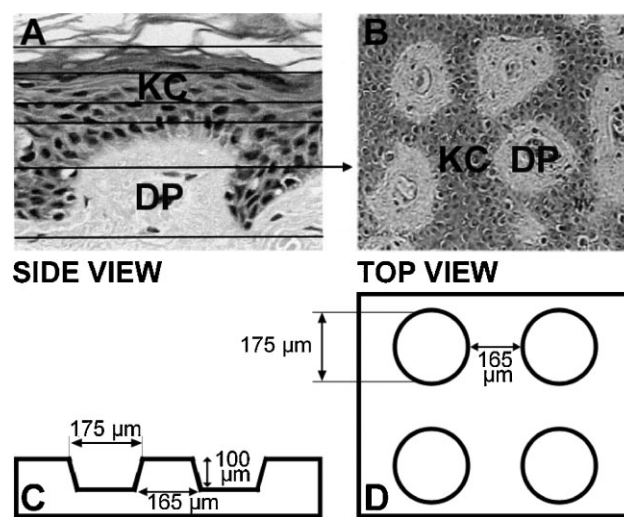


**Figure 2.** Design of the PDMS mold based on the architecture of the human papillary dermis. (A) Cross-section of normal human skin (inner forearm) showing the rete ridge architecture with keratinocytes (KC) and a dermal papilla (DP). (B) Top view of a longitudinal (*en face*) section at the height of the arrow in (A) showing the organization of the dermal papillae (DP). Dimensions were obtained from *in vivo* reflectance confocal microscopy measurements taken from ref.<sup>[12]</sup> (A,B) Adapted with permission from Macmillan Publishers Ltd., *The Journal of Investigative Dermatology*, © 2001.<sup>[12]</sup> (C) Side view and (D) top view of the PDMS casting mold design that was produced from a micromilled polycarbonate master.

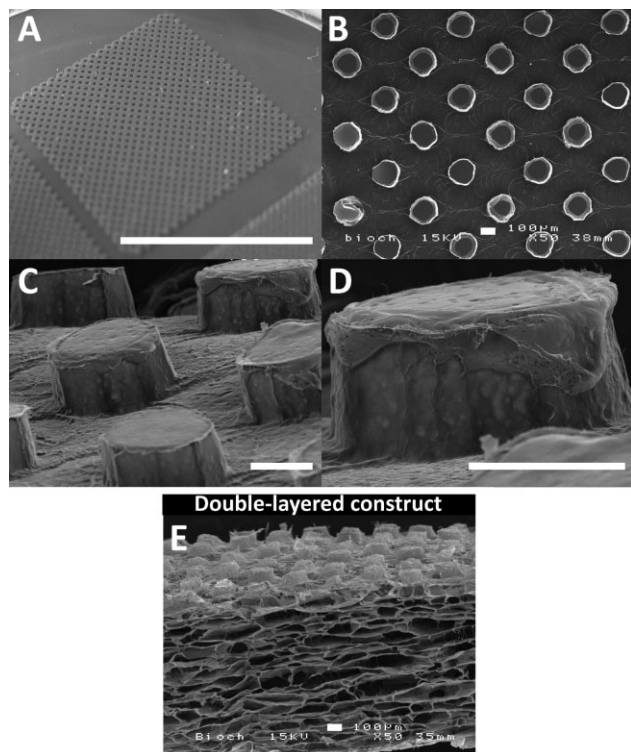


**Figure 3.** (A) Macroscopic picture of the microstructured PDMS mold and (B–E) scanning electron micrographs of papillary-structured collagen membranes produced with this mold. (B) Top view and (C) side view of a collagen membrane showing multiple papillar structures. (D) Close-up view of a single collagen papillar structure. (E) Double-layered collagen construct mimicking the two layers of the dermis: the papillary dermis (upper layer) and the reticular dermis (lower layer). Bar in (A) is 1 cm, bars in (B–E) are 100  $\mu\text{m}$ .

membranes adequately reflected the dimensions of the original design, thereby reproducing the natural morphology of dermal papillae.

The potential of creating a two-layered dermal substitute with a papillary dermis architecture combined with a porous reticular dermis layer was demonstrated (Figure 3E). For the two-layered construct, the papillary-structured membrane was prepared as described, but care was taken to prevent complete air-drying the collagen suspension on the mold. A fresh collagen suspension was poured on top of the slightly hydrated papillary-structured membrane, followed by freezing and lyophilization. This resulted in a porous construct mimicking the entire dermis with a papillary-structured semi-closed surface on top (Figure 3E).

## 2.2. Morphological Differences Related to Collagen Film Topography of Keratinocytes Cultured on Papillary-Structured Collagen Membranes

To investigate the effect of the papillary membrane architecture on cell growth and differentiation, primary

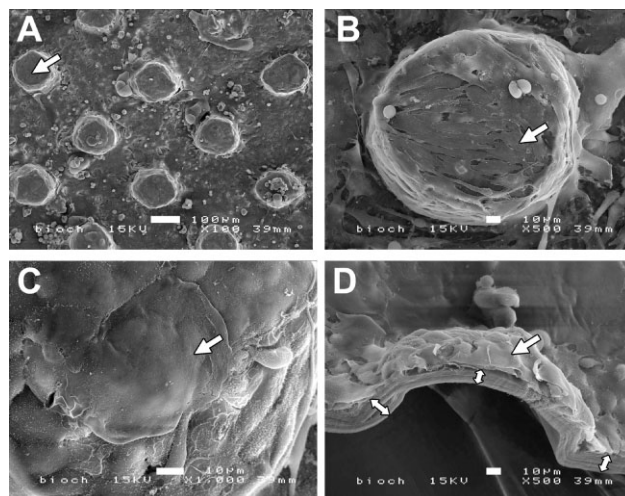


**Figure 4.** Scanning electron micrographs of human keratinocytes cultured on papillary-structured collagen membranes. Membranes were covered with a confluent layer of cells. (A) Top overview, (B) and (C) keratinocytes on a single papillar structure, (D) cross-sectional view of a single papillar structure. Typical cultured keratinocytes were visible (arrows). The collagen membrane in (D) is indicated with double arrow heads. Bars are (A) 100  $\mu\text{m}$  and (B–D) 10  $\mu\text{m}$ .

human keratinocytes were cultured submerged on papillary-structured and flat membranes.

Scanning electron microscopical analysis showed the presence of a confluent cell layer on both the papillary-structured and flat membranes (the papillary-structured membrane is shown in Figure 4). Cells showed the typical morphology of cultured keratinocytes and completely covered the membrane including the side and top of the papillar structures.

Staining of sections with toluidine blue and basic fuchsin showed the presence of predominantly a single layer of cells on the flat membranes and horizontal surfaces of the papillary-structured membranes (Figure 5A and B). At the base of the papillar structures, multiple cell layers were observed consisting of larger and more rounded cells, especially those in the corner regions.

Transmission electron microscopy confirmed these morphological differences (Figure 5C–F). The flat membranes and the horizontal parts of the papillary-structured membranes contained a single layer of cultured keratinocytes with their typical morphology (Figure 5C). Cells were closely attached to each other and contained intracellular keratin filaments and microvilli on top that extended into the cell culture medium. Melanin granules were visible, some subjected to autophagic fusion, which is known to occur in cultured keratinocytes.<sup>[29]</sup> A basement membrane was observed at the interface between the cells and the collagen membrane (Figure 5D). At the base of the papillar structures, the cultured sheet thickened up to about 6–7 cell

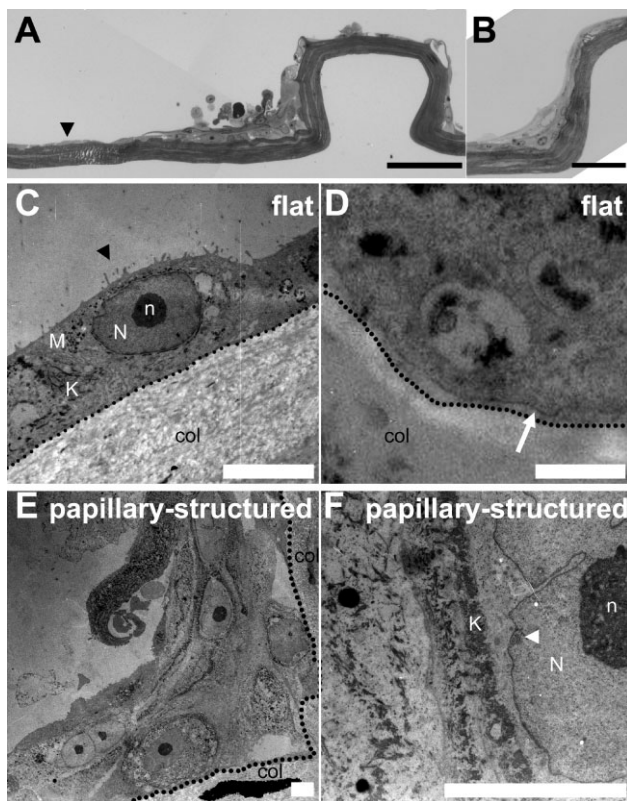


**Figure 5.** Morphology of keratinocytes cultured on papillary-structured and flat collagen membranes. A,B: Cross-sections of papillary-structured membranes with keratinocytes stained with toluidine blue and basic fuchsin. C–F: Electron microscopy of (C,D) flat and (E,F) papillary-structured membranes with keratinocytes. The horizontal parts of the membranes were covered with a single layer of flat keratinocytes [black arrowheads in (A) and (C)], while at the bottom of the papillar structures multiple layers of larger, more rounded cells were visible. Please note that (B) is derived from a pilot experiment where 75 000 cells were cultured on the membrane for 7 d in another culturing medium.<sup>[30]</sup> The dotted lines in C–E indicate the border between collagen membrane and cell layer. (C) Flat membranes were covered with a single layer of keratinocytes containing melanin granules and keratin filaments. (D) Higher magnification showing the basement membrane (thin line, arrow) of the keratinocytes. (E) At the base of the papillar structures up to 6–7 cell layers were present containing morphologically different cells. (F) The presence of keratin filaments (K) inside the cytoplasm of a cell with lobed nucleus demonstrates that this was also a keratinocyte, and the looping in the nuclear membrane (white arrowhead) is characteristic for young cells. N: nucleus, n: nucleolus, M: melanin granules, K: keratin filaments, col: collagen membrane. (A) is composed of two pictures. Scale bars in (A) and (B) are 100  $\mu\text{m}$ , bars in (C), (E), and (F) are 10  $\mu\text{m}$ , and bar in (D) is 1  $\mu\text{m}$ .

layers, containing morphologically diverse cells (Figure 5E). This included cells with the typical morphology of cultured keratinocytes, but also cells with a lobed nuclear membrane, and a mitochondria-rich and electron-light cytoplasm. Closer examination of these cells showed the

presence of keratin filaments peripheral in their cytoplasm (Figure 5F), confirming that these were also keratinocytes. Together with the observed nuclear membrane looping, which is characteristic for young cells, this demonstrated the presence of young keratinocytes at the base of the papillar structures.

### 2.3. Gene Expression Profile of Keratinocytes on Papillary-Structured Collagen Membranes

Gene expression microarrays provide an unbiased and comprehensive approach to gain insight into the nature of the different cells observed at different positions on the papillary-structured membrane (e.g., the morphological distinct cells observed at the base of the papillar structures vs. cells on flat surfaces). An attempt was made to separate cells associated with the papillar structures from cells associated with the flat surface in between the papillar structures, using laser dissection. Membranes cultured with keratinocytes were placed on crosslinked polyethylene naphthalate (PEN) membrane slides (Leica Microsystems, Wetzlar, Germany) and subjected to a Leica AS LMD microdissection system with a UV laser (Leica Microsystems). However, collagen membranes were too thick to cut out papillar structures without damaging the cultured cell layer. As an alternative, we compared RNA isolated from all the cells on the papillary-structured membranes to RNA isolated from cells on the flat membranes. Genes were ranked on their fold-change and of the 17 859 genes assessed, 88 were >1.5-fold higher expressed in keratinocytes cultured on papillary-structured membranes (Table 1A), and 168 were >1.5-fold higher expressed on flat membranes (Table 1B). It should be noted that since the papillary-structured membrane consists of both flat surfaces and papillar structures, specific gene profiles of cells of interest (e.g., those present at the base of the papillar structures) are diluted by the majority of associated flat surface. For instance, if cells at the base of papillar structures represent only 5% of the cell population, a  $21\times$  differential gene expression in these cells will only give a twofold change for the entire cell population. This probably explains the small fold-changes observed and the absence of statistical significance for the differentially expressed genes. However, this analysis nevertheless provided a valuable starting point for further analyses using reverse transcriptase quantitative PCR (RT-qPCR) and immunohistochemistry.

Gross examination of the gene lists provided a first indication of the nature of the differences between the cells on the two membranes. For example, the list of genes with higher expression on the papillary-structured membranes (Table 1A) contained three transmembrane tetraspanins, three interleukin (IL) receptors and two ILs, molecules generally associated with proliferation, which were all

**Table 1A.** List of all 88 genes  $> 1.5\times$  higher expressed in keratinocytes cultured on papillary-structured collagen membranes than on flat membranes.

No.	Gene symbol	Gene name	Fold change
1	TSPAN7	tetraspanin 7	2.7
2	C6orf155	chromosome 6 open reading frame 155	2.7
3	IL13RA2	interleukin 13 receptor, alpha 2	2.5
4	TAS2R4	taste receptor, type 2, member 4	2.2
5	TFPI2	tissue factor pathway inhibitor 2	2.1
6	CCBE1	collagen and calcium binding EGF domains 1	2.1
7	ZNF737	zinc finger protein 737	2.0
8	TAS2R20	taste receptor, type 2, member 20	2.0
9	PTGS2	prostaglandin endoperoxide synthase 2 (prostaglandin G/H synthase and cyclooxygenase)	2.0
10	ABI3BP	ABI family, member 3 (NESH) binding protein	2.0
11	IL24	interleukin 24	2.0
12	GSR	glutathione reductase	1.9
13	IFNE	interferon, epsilon	1.9
14	OC554202	hypothetical LOC554202	1.9
15	AMY2B	amylase, alpha 2B (pancreatic)	1.9
16	ANO1	anoctamin 1, calcium activated chloride channel	1.9
17	ABCC3	ATP-binding cassette, sub-family C (CFTR/MRP), member 3	1.8
18	NRCAM	neuronal cell adhesion molecule	1.8
19	IL1R2	interleukin 1 receptor, type II	1.8
20	LCP1	lymphocyte cytosolic protein 1 (L-plastin)	1.8
21	STEAP1	six transmembrane epithelial antigen of the prostate 1	1.8
22	RPL31	ribosomal protein L31	1.8
23	AKR1C1	aldo-keto reductase family 1, member C1 [dihydrodiol dehydrogenase 1; 20-alpha (3-alpha)-hydroxysteroid dehydrogenase]	1.8
24	CYP4F11	cytochrome P450, family 4, subfamily F, polypeptide 11	1.8
25	MRPS17	mitochondrial ribosomal protein S17	1.8
26	PTGS1	prostaglandin-endoperoxide synthase 1 (prostaglandin G/H synthase and cyclooxygenase)	1.8
27	C20orf197	chromosome 20 open reading frame 197	1.8
28	TRIM52	tripartite motif-containing 52	1.8
29	TSPAN4	tetraspanin 4	1.8
30	GUSBL2	glucuronidase, beta-like 2	1.8
31	SD17B7P2	hydroxysteroid (17-beta) dehydrogenase 7 pseudogene 2	1.7
32	TAGLN3	transgelin 3	1.7
33	MMP3	matrix metalloproteinase 3 (stromelysin 1, progelatinase)	1.7
34	DNAJB4	DnaJ (Hsp40) homolog, subfamily B, member 4	1.7
35	FBN2	fibrillin 2	1.7
36	PLA2G4A	phospholipase A2, group IVA (cytosolic, calcium-dependent)	1.7
37	CTNNA1	catenin (cadherin-associated protein), alpha-like 1	1.7
38	ACAT2	acetyl coenzyme A acetyltransferase 2	1.7
39	GPR39	G protein-coupled receptor 39	1.7
40	DKK1	dickkopf homolog 1 ( <i>Xenopus laevis</i> )	1.7

Table 1A. (Continued)

No.	Gene symbol	Gene name	Fold change
41	TFRC	transferrin receptor (p90, CD71)	1.7
42	ADAMTS6	ADAM metalloproteinase with thrombospondin type 1 motif, 6 (affymetrix transcript cluster 1)	1.7
43	POPDC3	popeye domain containing 3	1.7
44	ANKRD36B	ankyrin repeat domain 36B	1.7
45	WNT7B	wingless-type MMTV integration site family, member 7B	1.7
46	TUBA1B	tubulin, alpha 1b	1.6
47	C6orf105	chromosome 6 open reading frame 105	1.6
48	ADAMTS6	ADAM metalloproteinase with thrombospondin type 1 motif, 6 (affymetrix transcript cluster 2)	1.6
49	–		1.6
50	NRN1	neuritin 1	1.6
51	HSD17B2	hydroxysteroid (17-beta) dehydrogenase 2	1.6
52	QRFP	pyroglutamylated RFamide peptide	1.6
53	EVI2B	ecotropic viral integration site 2B	1.6
54	CTSK	cathepsin K	1.6
55	FGF2	FGF2 (basic)	1.6
56	PXN	paxillin	1.6
57	PMS2CL	PMS2 C-terminal like pseudogene	1.6
58	GOLGA8B	golgi autoantigen, golgin subfamily a, 8B	1.6
59	–		1.6
60	CYR61	cysteine-rich, angiogenic inducer, 61	1.6
61	OCLM	oculomedin	1.6
62	LOX	lysyl oxidase	1.6
63	AXL	AXL receptor tyrosine kinase	1.6
64	PHLDB2	pleckstrin homology-like domain, family B, member 2	1.6
65	TXNRD1	thioredoxin reductase 1	1.6
66	SLIT2	slit homolog 2 (drosophila)	1.6
67	FGF5	fibroblast growth factor 5	1.5
68	CMC1	COX assembly mitochondrial protein homolog ( <i>S. cerevisiae</i> )	1.5
69	RAB3B	RAB3B, member RAS oncogene family	1.5
70	EID3	EP300 interacting inhibitor of differentiation 3	1.5
71	MAP9	microtubule-associated protein 9	1.5
72	CAPRN2	caprin family member 2	1.5
73	FAM101A	family with sequence similarity 101, member A	1.5
74	SUZ12P	suppressor of zeste 12 homolog pseudogene	1.5
75	IL1RL1	interleukin 1 receptor-like 1	1.5
76	EFEMP1	EGF-containing fibulin-like extracellular matrix protein	1.5
77	NAV3	neuron navigator 3	1.5
78	–		1.5
79	TSPAN1	tetraspanin 1	1.5
80	IL6	interleukin 6 (interferon, beta 2)	1.5

Table 1A. (Continued)

No.	Gene symbol	Gene name	Fold change
81	C13orf15	chromosome 13 open reading frame 15	1.5
82	SPP1	secreted phosphoprotein 1	1.5
83	GLIS3	GLIS family zinc finger 3	1.5
84	ZNF675	zinc finger protein 675	1.5
85	RCN1	reticulocalbin 1, EF-hand calcium binding domain	1.5
86	PPP1R12B	protein phosphatase 1, regulatory (inhibitor) subunit 1	1.5
87	MME	membrane metallo-endopeptidase	1.5
88	BMS1P5	BMS1 pseudogene 5	1.5

absent from the list of genes with higher expression on the flat membranes (Table 1B). The first list also contained development-related genes like fibroblast growth factor 2 (basic) (FGF2), wntless-type MMTV integration site family, member 7B (WNT7B), and dickkopf homolog 1 (*Xenopus laevis*) (DKK1). In addition, fibrillin 2 (FBN2) was present, which is known to be expressed by keratinocytes and is probably involved in the development and maintenance of the elastic dermal-epidermal junction network.<sup>[31]</sup> The genes with higher expression on the flat membranes (Table 1B), on the other hand, were more related to keratinocyte differentiation, and contained, e.g., four late cornified envelope (LCE) genes. Other epithelia-related genes included keratins, beta 1 defensin (DEFB1), and cystatin E/M (CST6). However, complete terminal differentiation, for instance with respect to cytokeratins, was not observed possibly because a submerged, rather than an air-exposed, culture system was used.

#### 2.4. RT-qPCR Validation of Microarray Results

To validate the microarray results, RT-qPCR was performed on seven >1.3-fold differentially expressed genes selected for their reported association with skin biology (Figure 6),<sup>[18,23–26]</sup> including four upregulated genes [#40: dickkopf homolog 1 (*Xenopus laevis*) (DKK1); #80: IL 6 (interferon, beta 2) (IL6); #97: vanin 1 (VNN1); and #306: lumican (LUM)], and three downregulated genes [#33: late cornified envelope 2B (LCE2B); #34: defensin, beta 1 (DEFB1); and #35: cystatin E/M (CST6)]. All genes evaluated showed an up-/downregulation as indicated by the microarray results. Upregulation of DKK1 and downregulation of LCE2B and CST6 were statistically significant using this approach. These results indicate that despite the heterogeneity of the cell populations, the microarray findings reflect real changes in gene expression.

#### 2.5. Localization of Differentially Expressed Gene Products on Papillary-Structured Membranes

To investigate whether the observed changes in gene expression are related to the location of the cell on the collagenous membranes, the protein product of three >1.3-fold differentially expressed genes was visualized by immunohistochemical staining on cryosections of papillary-structured membranes (Figure 7).

Antibody staining for fibrillin 2 (upregulated #35) showed the presence of this protein on top of the papillar structures, while less staining was observed in the single cell layer on the flat part of the membrane between the papillar structures. In line with the microarray results, an association was observed between fibrillin 2 and the papillar structures, however, apparently not related to the morphologically distinct cells at the base of the structures, but at their top. Loricrin (downregulated #236) and cystatin E/M (downregulated #35) staining was found in almost all cells, but at the base of the papillar-structures where multiple cell layers were present, staining was less intense for the more basal cells in the corner. These differences in staining intensity support the microarray data.

#### 2.6. Pathway Analysis of Differentially Expressed Genes

To obtain more insight in the biological meaning of the microarray data, the differentially expressed genes (Table 1A and B) were analyzed for known direct interactions between their protein products (Figure 8A and B).

Of the 88 genes upregulated in keratinocytes on papillary-structured membranes, 27 had a known direct interaction with each other (Figure 8A). These proteins are mainly located at the plasma membrane or in the extracellular space. Key proteins in this network appear

**Table 1B.** List of all 168 genes > 1.5× higher expressed in keratinocytes cultured on flat membranes than on papillary-structured collagen membranes.

No.	Gene symbol	Gene name	Fold change
1	SPINK1	serine peptidase inhibitor, Kazal type 1	-3.8
2	-		-2.8
3	MPRSS11E	transmembrane protease, serine 11E	-2.5
4	DCT	dopachrome tautomerase (dopachrome delta-isomerase, tyrosine-related protein 2)	-2.3
5	PSG6	pregnancy specific beta-1-glycoprotein 6	-2.3
6	FAM70A	family with sequence similarity 70, member A	-2.3
7	BPIL2	bactericidal/permeability-increasing protein-like 2	-2.3
8	ELMOD1	ELMO/CED-12 domain containing 1	-2.2
9	XKRX	XK, Kell blood group complex subunit-related, X-linked	-2.2
10	CYP1A1	cytochrome P450, family 1, subfamily A, polypeptide 1	-2.2
11	SERPINA3	serpin peptidase inhibitor, clade A (alpha-1 antitrypsin, antitrypsin), member 3	-2.2
12	C12orf36	chromosome 12 open reading frame 36	-2.1
13	ACPP	acid phosphatase, prostate	-2.1
14	MLANA	melan-A	-2.1
15	STEAP4	STEAP family member 4	-2.1
16	IFIT1	interferon-induced protein with tetratricopeptide repeats 1	-2.1
17	OR10A3	olfactory receptor, family 10, subfamily A, member 3	-2.1
18	SEPT3	septin 3	-2.1
19	TPPP3	tubulin polymerization-promoting protein family member 3	-2.1
20	TYRP1	tyrosinase-related protein 1	-2.0
21	NEBL	nebulette	-2.0
22	ATP12A	ATPase, H+ /K+ transporting, nongastric, alpha polypeptide	-2.0
23	SILV	silver homolog (mouse)	-2.0
24	SPINK6	serine peptidase inhibitor, Kazal type 6	-2.0
25	KRT4	keratin 4	-2.0
26	MUC15	mucin 15, cell surface associated	-2.0
27	LIPH	lipase, member H	-2.0
28	ANKRD22	ankyrin repeat domain 22	-1.9
29	HSPB8	heat shock 22 kDa protein 8	-1.9
30	LCE1D	late cornified envelope 1D	-1.9
31	SERPINB4	serpin peptidase inhibitor, clade B (ovalbumin), member 4	-1.9
32	PSG4	pregnancy specific beta-1-glycoprotein 4	-1.9
33	LCE2B	late cornified envelope 2B	-1.9
34	DEFB1	defensin, beta 1	-1.9
35	CST6	cystatin E/M	-1.9
36	AZGP1	alpha-2-glycoprotein 1, zinc-binding	-1.9
37	SMPD3	sphingomyelin phosphodiesterase 3, neutral membrane (neutral sphingomyelinase II)	-1.9
38	CALB1	calbindin 1, 28 kDa	-1.9
39	ZNF750	zinc finger protein 750	-1.9
40	AQP9	aquaporin 9	-1.9
41	MX1	myxovirus (influenza virus) resistance 1, interferon-inducible protein p78 (mouse)	-1.9

Table 1B. (Continued)

No.	Gene symbol	Gene name	Fold change
42	IFI44L	interferon-induced protein 44-like	-1.9
43	ALDH3B2	aldehyde dehydrogenase 3 family, member B2	-1.9
44	TAS2R39	taste receptor, type 2, member 39	-1.9
45	EPHX3	epoxide hydrolase 3	-1.8
46	TYR	tyrosinase (oculocutaneous albinism IA)	-1.8
47	FOXP1	forkhead box N1	-1.8
48	CDRT1	CMT1A duplicated region transcript 1	-1.8
49	PSG9	pregnancy specific beta-1-glycoprotein 9	-1.8
50	SLC5A1	solute carrier family 5 (sodium/glucose cotransporter), member 1	-1.8
51	DSG4	desmoglein 4	-1.8
52	PDIA6	protein disulfide isomerase family A, member 6	-1.8
53	TTC39A	tetratricopeptide repeat domain 39A	-1.8
54	CLDN17	claudin 17	-1.8
55	GDA	guanine deaminase	-1.8
56	SCNN1B	sodium channel, nonvoltage-gated 1, beta	-1.8
57	USP2	ubiquitin specific peptidase 2	-1.8
58	KLK13	kallikrein-related peptidase 13	-1.8
59	TMEM86A	transmembrane protein 86A	-1.8
60	LCN2	lipocalin 2	-1.8
61	SLC39A2	solute carrier family 39 (zinc transporter), member 2	-1.8
62	PLA2G4E	phospholipase A2, group IVE	-1.7
63	CPA4	carboxypeptidase A4	-1.7
64	TMPRSS4	transmembrane protease, serine 4	-1.7
65	RSAD2	radical S-adenosyl methionine domain containing 2	-1.7
66	KLK14	kallikrein-related peptidase 14	-1.7
67	FAM83C	family with sequence similarity 83, member C	-1.7
68	MPRSS11F	transmembrane protease, serine 11F	-1.7
69	LCE2D	late cornified envelope 2D	-1.7
70	RDH12	retinol dehydrogenase 12 (all-trans/9-cis/11-cis)	-1.7
71	PLA2G7	phospholipase A2, group VII (platelet-activating factor acetylhydrolase, plasma)	-1.7
72	SLC6A14	solute carrier family 6 (amino acid transporter), member 14	-1.7
73	UQCRC1	ubiquinol-cytochrome c reductase, Rieske iron-sulfur polypeptide 1	-1.7
74	TNFSF10	tumor necrosis factor (ligand) superfamily, member 10	-1.7
75	LY6G6C	lymphocyte antigen 6 complex, locus G6C	-1.7
76	TXNIP	thioredoxin interacting protein	-1.7
77	RAET1L	retinoic acid early transcript 1L	-1.7
78	SPINK7	serine peptidase inhibitor, kazal type 7 (putative)	-1.7
79	TRIM48	tripartite motif-containing 48	-1.7
80	CXCL14	chemokine (C-X-C motif) ligand 14	-1.7
81	BMP6	bone morphogenetic protein 6	-1.7
82	RGS2	regulator of G-protein signaling 2, 24 kDa	-1.7

Table 1B. (Continued)

No.	Gene symbol	Gene name	Fold change
83	IFI27	interferon, alpha-inducible protein 27	-1.7
84	MT1G	metallothionein 1G	-1.7
85	KRT78	keratin 78	-1.7
86	BBOX1	butyrobetaine (gamma), 2-oxoglutarate dioxygenase (gamma-butyrobetaine hydroxylase) 1	-1.7
87	CYP4B1	cytochrome P450, family 4, subfamily B, polypeptide 1	-1.7
88	NDUFA4L2	NADH dehydrogenase (ubiquinone) 1 alpha subcomplex, 4-like 2	-1.7
89	PI15	peptidase inhibitor 15	-1.7
90	HIST1H4H	histone cluster 1, H4 h	-1.7
91	GRHL1	grainyhead-like 1 (Drosophila)	-1.7
92	CCL22	chemokine (C-C motif) ligand 22	-1.6
93	EGR3	early growth response 3	-1.6
94	OCA2	oculocutaneous albinism II	-1.6
95	KRT80	keratin 80	-1.6
96	OBP2B	odorant binding protein 2B	-1.6
97	PDZK1IP1	PDZK1 interacting protein 1	-1.6
98	TMPRSS13	transmembrane protease, serine 13	-1.6
99	SCNN1A	sodium channel, nonvoltage-gated 1 alpha	-1.6
100	GSTP1	glutathione S-transferase theta pseudogene 1	-1.6
101	CYP1B1	cytochrome P450, family 1, subfamily B, polypeptide 1	-1.6
102	EDNRB	endothelin receptor type B	-1.6
103	PVRL4	poliovirus receptor-related 4	-1.6
104	RPL23AP32	ribosomal protein L23a pseudogene 32	-1.6
105	IFIT3	interferon-induced protein with tetratricopeptide repeats 3	-1.6
106	OPN4	opsin 4	-1.6
107	NOV	nephroblastoma overexpressed gene	-1.6
108	OAS1	2',5'-oligoadenylate synthetase 1, 40/46 kDa	-1.6
109	CLIC3	chloride intracellular channel 3	-1.6
110	PGLYRP3	peptidoglycan recognition protein 3	-1.6
111	ATG9B	ATG9 autophagy related 9 homolog B (S. cerevisiae)	-1.6
112	OAS2	2'-5'-oligoadenylate synthetase 2, 69/71 kDa	-1.6
113	CAMK1D	calcium/calmodulin-dependent protein kinase ID	-1.6
114	RAB27B	RAB27B, member RAS oncogene family	-1.6
115	CCNA1	cyclin A1	-1.6
116	MUCL1	mucin-like 1	-1.6
117	FLVCR2	feline leukemia virus subgroup C cellular receptor family, member 2	-1.6
118	CXCL11	chemokine (C-X-C motif) ligand 11	-1.6
119	TMEM45B	transmembrane protein 45B	-1.6
120	SPRR2C	small proline-rich protein 2C (pseudogene)	-1.6
121	CLDN7	claudin 7	-1.6
122	POF1B	premature ovarian failure, 1B	-1.6

Table 1B. (Continued)

No.	Gene symbol	Gene name	Fold change
123	SCEL	sciellin	-1.6
124	OVOL1	ovo-like 1(Drosophila)	-1.6
125	TRIM16	tripartite motif-containing 16	-1.6
126	SAMD9	sterile alpha motif domain containing 9	-1.6
127	ABCG1	ATP-binding cassette, sub-family G (WHITE), member 1	-1.6
128	MPZL3	myelin protein zero-like 3	-1.6
129	HIST1H2BK	histone cluster 1, H2bk	-1.6
130	SLC24A5	solute carrier family 24, member 5	-1.6
131	KLK6	kallikrein-related peptidase 6	-1.6
132	TRIM2	tripartite motif-containing 2	-1.6
133	POTEE	POTE ankyrin domain family, member E	-1.6
134	GGT6	gamma-glutamyltransferase 6	-1.6
135	TCP11L2	t-complex 11 (mouse)-like 2	-1.6
136	GPR110	G protein-coupled receptor 110	-1.6
137	KRT23	keratin 23 (histone deacetylase inducible)	-1.6
138	SULT2B1	sulfotransferase family, cytosolic, 2B, member 1	-1.6
139	PSG8	pregnancy specific beta-1-glycoprotein 8	-1.6
140	GRHL3	grainyhead-like 3 (Drosophila)	-1.6
141	ERBB3	v-erb-b2 erythroblastic leukemia viral oncogene homolog 3	-1.6
142	IGFBP5	insulin-like growth factor binding protein 5	-1.6
143	CLIC5	chloride intracellular channel 5	-1.6
144	FKBP9	FK506 binding protein 9, 63 kDa	-1.6
145	PGLYRP4	peptidoglycan recognition protein 4	-1.6
146	C6orf35	chromosome 6 open reading frame 35	-1.5
147	PLEKHA7	pleckstrin homology domain containing, family A member 7	-1.5
148	CA9	carbonic anhydrase IX	-1.5
149	BMP4	bone morphogenetic protein 4	-1.5
150	ATP10B	ATPase, class V, type 10B	-1.5
151	GALNT5	UDP-N-acetyl- $\alpha$ -D-galactosamine:polypeptide N-acetylgalactosaminyltransferase 5 (GalNAc-T5)	-1.5
152	CRABP2	cellular retinoic acid binding protein 2	-1.5
153	LCE2A	late cornified envelope 2A	-1.5
154	DGAT2	diacylglycerol O-acyltransferase homolog 2 (mouse)	-1.5
155	MAFB	v-maf musculoaponeurotic fibrosarcoma oncogene homolog B (avian)	-1.5
156	GMPR	guanosine monophosphate reductase	-1.5
157	SBSN	suprabasin	-1.5
158	CYP2F1	cytochrome P450, family 2, subfamily F, polypeptide 1	-1.5
159	KRT13	keratin 13	-1.5
160	TGM1	transglutaminase 1 (K polypeptide epidermal type I, protein-glutamine-gamma-glutamyltransferase)	-1.5
161	TIAM1	T-cell lymphoma invasion and metastasis 1	-1.5

Table 1B. (Continued)

No.	Gene symbol	Gene name	Fold change
162	CCBP2	chemokine binding protein 2	-1.5
163	CEBPA	CCAAT/enhancer binding protein (C/EBP), alpha	-1.5
164	FLJ13744	hypothetical FLJ13744	-1.5
165	BNIP1	BCL2/adenovirus E1B 19 kD interacting protein like	-1.5
166	AADACL2	arylacetamide deacetylase-like 2	-1.5
167	RHCG	Rh family, C glycoprotein	-1.5
168	RAB11FIP1	RAB11 family interacting protein 1 (class I)	-1.5

to be FGF2, IL 6 (IL6), group IV A phospholipase A2 (PLA2G4A), and prostaglandin-endoperoxide synthase 2 (PTGS2).

Of the 168 genes upregulated in keratinocytes on flat membranes, 32 directly interacted with each other

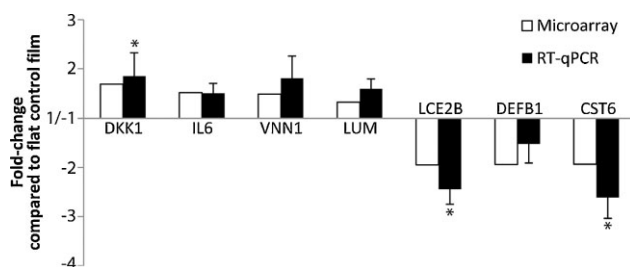


Figure 6. RT-qPCR validation of differentially expressed genes in keratinocytes on papillary-structured membranes compared to flat membranes. Depicted are the fold-changes identified with the gene expression microarrays (open bars) and their validation using RT-qPCR (filled bars) ± S. E. M. An asterisk (\*) indicates statistically significant changes on papillary-structured versus flat membranes ( $p < 0.05$ ).

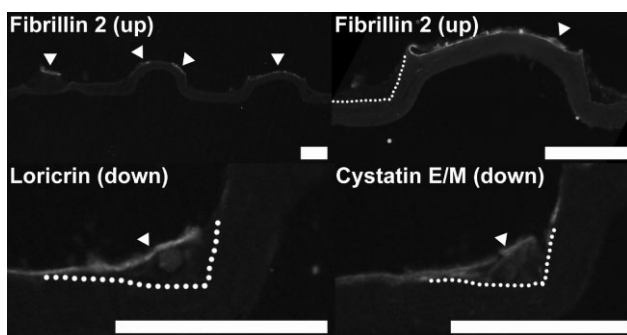
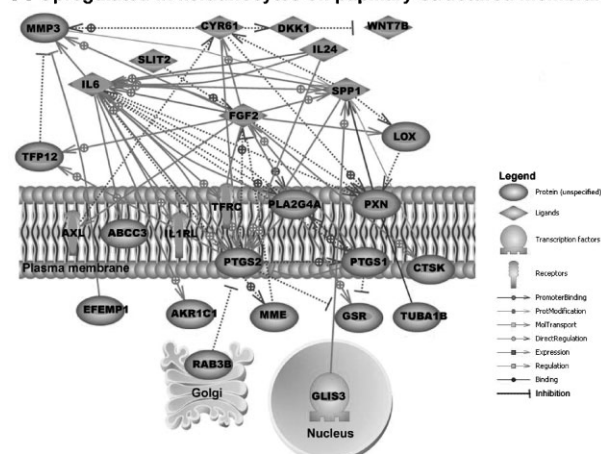


Figure 7. Visualization of proteins (arrowheads) from differentially expressed genes on papillary-structured membranes with keratinocytes. Staining for fibrillin 2 (upregulated on papillary-structured membranes), and loricrin and cystatin E/M (down-regulated on papillary-structured membranes). The dotted line indicates a part of the border between the collagen membrane and cultured cell layer. Bars are 50  $\mu\text{m}$ .

(Figure 8B). Key players in this network are (i) the transcription factor CCAAT/enhancer binding protein alpha (CEBPA) involved in differentiation and in mitotic growth arrest and (ii) tyrosinase (oculocutaneous albinism IA) (TYR) in another part of the network.

A Upregulated in keratinocytes on papillary-structured membranes



B Upregulated in keratinocytes on flat membranes

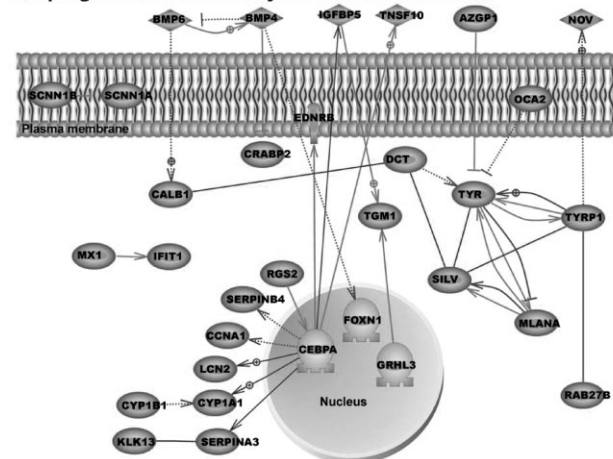


Figure 8. Pathway analysis of (A) the genes upregulated in keratinocytes on papillary-structured membranes and (B) upregulated in keratinocytes on flat membranes.

### 3. Discussion

A collagen membrane matching the natural architecture of the human skin's basement membrane was constructed, by mimicking the topology of dermal papillae. Cultured keratinocytes were able to establish a confluent layer. In contrast to the single layered keratinocytes on the flat part of the membrane, multiple layers were present at the base of the papillary structures, containing morphologically distinct cells including young keratinocytes. This provided a first indication that the membrane architecture could result in a direct biological effect on the cultured cells. Microarray analysis was used as an unbiased and comprehensive tool to obtain insight in the differences between keratinocytes on papillary-structured and flat membranes. The gene expression profiles obtained hinted to specific cell behavior, and expression levels were validated by RT-qPCR, indicating that the observed differences in gene expression reflect real changes. This was confirmed by antibody staining for a number of proteins encoded by the differentially expressed genes. Thus, despite the initial concerns that differences could be diluted out, significant differences were found.

The list of upregulated genes on papillary-structured membranes contained genes known to be involved in cell signaling, development, and proliferation. Pathway analysis provided more insight in the biological nature of the differences in gene expression. The protein products of genes upregulated on papillary-structured membranes were mainly situated on the plasma membrane and in the extracellular space. The key proteins in this network have been reported to be involved in keratinocyte proliferation and migration. FGF2, for example, stimulates keratinocyte proliferation.<sup>[32]</sup> IL 6 can indirectly induce keratinocyte migration.<sup>[26]</sup> In addition, group IV A phospholipase A2 (PLA2G4A) and PTGS2 [also known as cyclooxygenase 2 (COX-2)] are both required for the conversion of cell membrane phospholipids into prostaglandins that are involved in keratinocyte migration and proliferation.<sup>[33]</sup> Fibrillins form microfibrils that act as a scaffold for elastin, and in skin fibrillin 2 is mainly found at the dermal-epidermal junction.<sup>[34,35]</sup> In our study, fibrillin 2 was found on top of the papillary structures resembling the top of dermal papillae. Since the protein was not found at the horizontal surfaces between the structures, it is possible that these cells on top experienced a distinct tension (stress) that stimulated fibrillin deposition. Very clearly, the cells sense their local microenvironment. The interplay of topological cues and intercellular communication will be subject of more detailed future studies.

The list of genes upregulated on flat membranes contained a remarkable number of genes related to keratinocyte differentiation. Pathway analysis showed a more intracellular localization of the gene products. The central transcription factor of one part of the network,

C/EBPalpha is known for its role in keratinocyte terminal differentiation.<sup>[36]</sup> Proteins of the other part of the network, including tyrosinase (TYR), dopachrome tautomerase (DCT), and tyrosinase-related protein 1 (TYRP1), are known to be involved in the process of melanogenesis.<sup>[37]</sup>

In this study, only type I collagen was used as a matrix for cell growth. To mimic the natural basement membrane present between keratinocytes and the dermis, the papillary membrane may also be covered with basement membrane components such as type IV collagen and glycosaminoglycans. In addition, elastin may be included in the dermal structure, since it has been shown to stimulate keratinocyte proliferation.<sup>[30]</sup> Future research may also include the evaluation of keratinocytes cultured at the air/liquid interface, better representing the natural environmental conditions of keratinocytes. These additional experiments will probably lead to a better understanding of the direct effect of membrane architecture on keratinocyte behavior.

### 4. Conclusion

A collagen membrane representing the natural architecture of the dermal papillae in human skin was constructed. Cellular morphology, gene expression signatures and protein expression of keratinocytes cultured on these membranes were different when compared to flat membranes. This indicates that cellular characteristics can be directed by physical modification of biomaterials, which may form specific cellular niches. This knowledge may be used for the construction of improved tissue-engineered skin constructs.

## 5. Experimental Section

### 5.1. Design and Construction of the Papillary-Structured Mold

A papillary-structured mold was designed, implementing dimensions extracted from a published *in vivo* analysis of human skin using near-infrared confocal microscopy (Figure 2).<sup>[12]</sup> Dimensions of the inner forearm dermal papilla were deduced from histological pictures and quantitative data presented in this publication and a mold was designed to produce collagen membranes containing cones (microstructures) of 100  $\mu\text{m}$  height and 175  $\mu\text{m}$  width at the base, and an intercone distance of  $\approx 165 \mu\text{m}$ .

The collagen mold is made from a PDMS structure. The generation of PDMS masters as molds of a microstructured polycarbonate master is a typical work flow in the manufacturing of microfluidic systems or microstructured foils and thin films.<sup>[13]</sup> For master fabrication, a 115 mm diameter and 4 mm thick polycarbonate disk was machined using a Minitech Mini-Mill 3PRO 3-Axis CNC milling machine (Norcross, GA, USA) and a 15° V-shaped engraving bit with 100  $\mu\text{m}$  tip width to remove all

material except the intended cones. A spindle turning speed of 50 000 rpm and a feed rate of  $600 \text{ mm} \cdot \text{min}^{-1}$  was applied. Vertical and horizontal milling paths were constructed in a defined pattern using Autodesk AutoCAD 2007.

The PDMS molding was realized as casted resin by molding an addition-curing two component PDMS (Elastosil RT 607, Wacker, Munich, Germany) from the polycarbonate master in a brass form of an hot embossing machine (Schmidt Technology, Cranberry Twp., PA, USA). Elastosil components A and B were mixed at a 9:1 weight ratio at room temperature. The mixture was degassed in a desiccator and then poured onto the polycarbonate master in the brass form. The form was put into the hot embossing machine and pressed for 30 min under vacuum at  $80^\circ\text{C}$  to solidify. After demolding, the PDMS was washed with 100% ethanol. The final template for the construction of papillary-structured collagen membranes was thus a  $12 \times 12 \text{ mm}^2$  PDMS mold containing slightly sloped, cone shaped holes of  $175 \mu\text{m}$  width and  $100 \mu\text{m}$  depth, with an in between distance of  $165 \mu\text{m}$  (Figure 2C and D).

## 5.2. Production of Papillary-Structured and Flat Collagen Membranes

Type I collagen fibrils were purified from bovine Achilles tendon using extractions with diluted acetic acid, aqueous NaCl and urea, and acetone.<sup>[14]</sup> A suspension of collagen fibrils (0.8% w/v in 0.25 M acetic acid) was shaken overnight at  $4^\circ\text{C}$  and homogenized on ice using a Potter-Elvehjem homogenizer (Louwers Glass and Ceramic Technologies, Hapert, The Netherlands) with an intervening space of 0.35 mm until homogenization was completed. Air-bubbles were removed by centrifugation at 250 g for 10 min at  $4^\circ\text{C}$ . To obtain a container, a 35 mm Petri dish with the bottom removed was fixed on the papillary-structured PDMS cast and filled with collagen suspension (2 mL). Air entrapped in the indentations was removed by placing the cast with collagen suspension in a vacuum desiccator for  $3 \times 1 \text{ min}$ . The suspension was air-dried at room temperature. As a control, flat collagen membranes were produced on an adjacent surface of non-structured PDMS cast, using the same procedure.

For morphological analysis, the papillary-structured and flat membranes were mounted on stubs, sputtered with an ultrathin layer of gold in a Polaron E5100 coating system and visualized with a JEOL JSM-6310 scanning electron microscope (Tokyo, Japan) operating at 15 kV.

## 5.3. Production of a Papillary-Structured Double-Layered Construct

To demonstrate the feasibility of preparing a composite dermal substitute composed of a papillary dermal and a reticular dermal component, the papillary-structured papillary membrane was combined with a porous (dermal) scaffold. A collagen fibril suspension was poured on the papillary-structured PDMS cast (see Section 5.2.), and air-dried for 8 h resulting in near dry membranes. This layer was covered with collagen suspension (2 mL, resulting in a 1–2 mm layer), directly frozen at  $-20^\circ\text{C}$ , and lyophilized.

This double-layered construct was analyzed by scanning electron microscopy (see Section 5.2.).

## 5.4. Culture of Primary Human Keratinocytes on Papillary-Structured Membranes

Keratinocytes were obtained from human abdominal skin derived from donors who underwent surgery for abdominal wall correction.<sup>[15]</sup> Three papillary-structured and three flat membranes were evaluated. To ensure that seeded cells remained on top of the membranes, films were placed in 10 mm diameter CellCrown24 inserts (ScaffDex, Tampere, Finland), disinfected with 70% ethanol ( $3 \times 1 \text{ h}$  and  $1 \times 16 \text{ h}$ ), washed with sterile phosphate-buffered saline (pH = 7.2,  $5 \times 1 \text{ h}$ , and  $1 \times 16 \text{ h}$ ), placed on the bottom of a 6-well plate and pre-incubated for 16 h in keratinocyte growth medium (KGM).<sup>[16]</sup> Cells were seeded at a density of 100 000 cells/insert and incubated in medium (2 mL per well) at  $37^\circ\text{C}$  and 5%  $\text{CO}_2$ . Cells were cultured to confluency on the membranes for 10 d and medium was refreshed on day 3 and 6. Membranes + cells were removed from the inserts, divided in two and processed for microscopical evaluation and RNA analysis.

## 5.5. Microscopic Evaluation

One half of the membranes with cultured keratinocytes was rinsed with phosphate buffer (PB, 0.1 M, pH = 7.4), fixed with paraformaldehyde (4% in 0.1 M PB) for 30 min at room temperature, washed with PB (0.1 M), and divided in three pieces for (electron) microscopical evaluation and (immuno)cytochemistry.

For scanning electron microscopy, one piece was dehydrated in an ascending graded series of ethanol up to 100% ethanol, critical point dried using  $\text{CO}_2$  with a Polaron E3000 critical point drying apparatus (Watford, UK), processed and visualized with a JEOL JSM-6310.

For light and transmission microscopy, one piece was further fixed in glutaraldehyde [2% in 0.1 M phosphate buffer (pH = 7.4)], post-fixed with osmium tetroxide (1%), dehydrated in an ascending series of ethanol, and embedded in Epon 812. To obtain a general overview by light microscopy,  $1 \mu\text{m}$  sections were stained with toluidine blue and basic fuchsin. For a more detailed analysis, ultrathin sections (60 nm) were cut and picked up on Formvar-coated grids, post-stained with lead citrate and uranyl acetate, and examined in a JEOL 1010 electron microscope.

For immunocytochemical evaluation, a third piece of the fixed membrane part was placed in TissueTek (Sakura Finetek, Zoeterwoude, The Netherlands), frozen in liquid nitrogen-cooled isopentane and sectioned. Cryosections were incubated in rabbit anti-human fibrillin 2 (1:200),<sup>[17]</sup> rabbit anti-human loricrin [1:500, Berkeley Antibody Company (BAbCO), Richmond, CA, USA], and rabbit anti-human cystatin M/E (1:200),<sup>[18]</sup> followed by an Alexa 488-labeled goat anti-rabbit IgG antibody (Molecular Probes, Eugene, OR, USA).<sup>[19]</sup>

## 5.6. RNA Isolation

The other unprocessed half of the membrane with cultured keratinocytes was placed directly in Qiagen lysis buffer RLT ( $350 \mu\text{A}$ ) for RNA isolation, vortexed for 1 min, and processed according to the Qiagen RNeasy mini kit protocol for the purification of total RNA from animal cells using spin technology (Qiagen, Hilden, Germany), including an on-column DNase

digestion. The RNA concentration and purity were measured with a Nanodrop spectrophotometer (Thermo Scientific, Waltham, MA, USA) and RNA integrity was analyzed on an Agilent Bioanalyser (Santa Clara, CA, USA). Per half of a membrane, 1.5–8  $\mu\text{g}$  RNA was isolated with an RNA integrity number (RIN) between 8.7 and 9.6, indicating excellent RNA quality.

### 5.7. High-Density Gene Expression Microarray Analysis

A comprehensive gene expression analysis was performed of keratinocytes cultured on papillary-structured and on flat membranes using high density gene expression microarrays. Microarray analysis was performed as described before, with minor modifications.<sup>[20]</sup> From the isolated total RNA, 100 ng was further processed according to the Affymetrix GeneChip whole transcript sense target labeling assay manual (Affymetrix, Santa Clara, CA, USA). First, the ribosomal RNA content was reduced using the Invitrogen RiboMinus transcriptome isolation kit. Then, double-stranded complementary DNA (cDNA) was synthesized from RNA, which was used for in vitro transcription, creating complementary RNA. This RNA was then used to create fluorescently labeled single-stranded DNA fragments in the sense orientation, which was hybridized on Affymetrix GeneChip human exon 1.0 sense target (ST) microarrays. These microarrays contain defined spots of oligonucleotide probes targeting a specific nucleotide sequence. Four spots with different probes form (in 90% of the cases) a probe set, covering every known and putative exon of the human genome. Using current annotation data, the 1.4 million probe sets (exons) on this array can be combined to analyze the expression of 17 859 individual genes.

The arrays were scanned and converted to a processed image, which was converted to one fluorescence intensity value per probe, using Affymetrix GeneChip Operating Software (GCOS). The values of individual probes belonging to one probe set were averaged using Partek Genomics Suite 6.4 (Partek Inc., St. Louis, MO, USA, www.partek.com). The average fluorescence intensity of all 17 859 genes on the microarrays was calculated using the Robust

Multiarray Analysis (RMA) algorithm,<sup>[21]</sup> including a quantile normalization and background correction for GC-content. Human genome version HG18 was used for annotation.<sup>[22]</sup>

To identify differentially expressed genes, a one-way analysis of variance (ANOVA) was performed for gene expression in keratinocytes cultured on papillary-structured versus flat membranes. Gene lists of interest were analyzed for known direct interactions between their gene products using Pathway studio 7.1 software (Ariadne, Rockville, MD, USA).

### 5.8. RT-qPCR Validation

Microarray data were validated by reverse transcriptase quantitative polymerase chain reaction (RT-qPCR) on skin-related genes.<sup>[18,23–26]</sup> For this 170 ng RNA was converted to cDNA using an Invitrogen SuperScript III first-strand synthesis system kit for RT-PCR by incubation at 65 °C for 5 min in the presence of random hexamers (50 ng) and deoxynucleotide triphosphate (dNTP,  $10^{-3}$  M) mix. After incubation on ice, the reaction mix was diluted 1:1 to a total volume of 20  $\mu\text{L}$  containing  $\text{MgCl}_2$  ( $5 \times 10^{-3}$  M), dithiothreitol (DTT, 0.01 M), RNaseOUT (40 U), and SuperScript III Reverse Transcriptase [200 U in 0.020 M Tris-HCl (pH = 8.4), and 0.050 M KCl]. This mixture was incubated for 10 min at 25 °C, and cDNA was synthesized for 50 min at 50 °C. Reaction was terminated at 85 °C for 5 min, placed on ice, and samples were stored at –20 °C.

In a 20  $\mu\text{L}$  reaction, 1 ng cDNA was mixed with SYBR green 2  $\times$  supermix (10  $\mu\text{L}$ , Bio-Rad), forward (12 pmol) and reverse (12 pmol) primers (Table 2). RT-qPCR was performed in a Bio-Rad (Hercules, CA, USA) C1000 thermal cycler with a CFX96 real-time PCR detection system using a hot start at 50 °C for 2 min and 95 °C for 10 min, followed by 40 cycles of 95 °C for 15 s, 60 °C for 1 min, including a plate read after every cycle, followed by 95 °C for 15 s, and a melt curve from 60 to 95 °C, incrementing 0.5 °C every 5 s accompanied by a plate read.

The cycle in which the fluorescence intensity passed a threshold ( $C_t$ ) was determined using Bio-Rad CFX manager. The  $\Delta C_t$  of a sample was then calculated by subtraction of the  $C_t$  value of the reference gene large ribosomal protein P0 (RPLP0) from the  $C_t$  value of the gene of interest. To calculate the  $\Delta C_t$ , the average  $\Delta C_t$  of

Table 2. Primer sequences and amplicon size of the genes assessed by RT-qPCR.

Primer name	Gene symbol	Forward primer (5'-3')	Reverse primer (5'-3')	Amplicon size (bp)
dickkopf homolog 1(Xenopus laevis)	<b>DKK1</b>	atcatagcaccttgatgggtatt	cttctgtcctttggtgtgatacattt	75
interleukin 6 (interferon, beta 2)	<b>IL6</b>	agccctgagaaaggagacatgta	ggcaagtctcctcattgaatcc	140
vanin 1 <sup>[28]</sup>	<b>VNN1</b>	gaaccagtagtctttcct	catacaacctcccaaacaga	147
lumican	<b>LUM</b>	cttcaatcagatagccagactgc	agccagttcgtgtgagataaac	151
late cornified envelope 2B <sup>[23]</sup>	<b>LCE2B</b>	ggttgactaaactctgccagg	cactggggcaggcattta	128
defensin, beta 1 <sup>[25]</sup>	<b>DEFB1</b>	atggcctcaggtgtaactttc	cacttggccttccctctgtaac	146
cystatin E/M <sup>[24]</sup>	<b>CST6</b>	tccgagacacgcacatcatc	ccatctccatcgtcaggaagtac	75
ribosomal protein, large, P0 (reference gene) <sup>[24,28]</sup>	<b>RPLP0</b>	caccattgaaatcctgagtgatgt	tgaccagcccaaggagaag	116

keratinocytes cultured on flat membranes was subtracted from the average  $\Delta C_t$  of keratinocytes cultured on papillary-structured membranes. The fold change was calculated as  $2^{-\Delta C_t}$ . RT-qPCR products were checked on agarose gel and were of expected size. To identify statistically significant changes in gene expression, an unpaired *t*-test was performed on the  $2^{-\Delta C_t}$  values of the individual genes assessed on papillary-structured versus flat membranes, and  $p < 0.05$  was considered significant.<sup>[27]</sup>

**Acknowledgements:** We like to thank Dr. Magda Ulrich and Prof. Dr. Esther Middelkoop of the Association of Dutch Burn Centers for their help with the porcine wound model (Figure 1). The MIC facility of the NCMLS is acknowledged for the use of the scanning electron microscope and cryostat, and we would like to express our gratitude to Paul Jap for the interpretation of TEM micrographs. We would like to thank Marcel Nelen and Suzanne Keijzers-Vloet of the Microarray Facility (Dept. of Human Genetics) for their assistance, and Henry Dijkman (Dept. of Pathology), and Peter Uijtdewilligen (Dept. of Biochemistry) for the use and their assistance in the laser microdissection pilot, respectively. This study is funded by the Dutch Program for Tissue Engineering (grant DPTE 6735 and 6739) and by the EU-FP6 project EuroSTEC (soft tissue engineering for congenital birth defects in children: contract: LSHB-CT-2006-037409).

Received: September 1, 2011; Revised: December 2, 2011;  
Published online: March 13, 2012; DOI: 10.1002/mabi.201100443

**Keywords:** biomedical applications; biomimetics; microstructures; tissue engineering

- [1] G. C. Gurtner, S. Werner, Y. Barrandon, M. T. Longaker, *Nature* **2008**, *453*, 314.
- [2] S. MacNeil, *Nature* **2007**, *445*, 874.
- [3] A. D. Metcalfe, M. W. Ferguson, *Biomaterials* **2007**, *28*, 5100.
- [4] U. B. Jensen, S. Lowell, F. M. Watt, *Development* **1999**, *126*, 2409.
- [5] R. M. Lavker, T. T. Sun, *Science* **1982**, *215*, 1239.
- [6] S. Ghazizadeh, L. B. Taichman, *J. Invest. Dermatol.* **2005**, *124*, 367.
- [7] S. Muffler, H. J. Stark, M. Amoros, B. Falkowska-Hansen, K. Boehnke, H. J. Buhning, A. Marme, J. R. Bickenbach, P. Boukamp, *Stem Cells* **2008**, *26*, 2506.
- [8] C. Pincelli, A. Marconi, *J. Cell Physiol.* **2010**, *225*, 310.
- [9] G. D. Pins, M. Toner, J. R. Morgan, *FASEB J.* **2000**, *14*, 593.
- [10] R. G. Flemming, C. J. Murphy, G. A. Abrams, S. L. Goodman, P. F. Nealey, *Biomaterials* **1999**, *20*, 573.
- [11] T. Steinberg, S. Schulz, J. P. Spatz, N. Grabe, E. Mussig, A. Kohl, G. Komposch, P. Tomakidi, *Nano Lett.* **2007**, *7*, 287.
- [12] M. Huzaira, F. Rius, M. Rajadhyaksha, R. R. Anderson, S. Gonzalez, *J. Invest. Dermatol.* **2001**, *116*, 846.
- [13] M. Focke, D. Kosse, C. Muller, H. Reinecke, R. Zengerle, S. F. von Stetten, *Lab Chip.* **2010**, *10*, 1365.
- [14] J. S. Pieper, A. Oosterhof, P. J. Dijkstra, J. H. Veerkamp, T. H. van Kuppevelt, *Biomaterials* **1999**, *20*, 847.
- [15] G. Tjabringa, M. Bergers, R. D. van Rens, B. R. de Boer, E. Lamme, J. Schalkwijk, *Am. J. Pathol.* **2008**, *173*, 815.
- [16] F. Van Ruissen, P. E. van Erp, G. J. de Jongh, J. B. Boezeman, P. C. van de Kerkhof, J. Schalkwijk, *J. Cell Sci.* **1994**, *107*, 2219.
- [17] G. Lin, K. Tiedemann, T. Vollbrandt, H. Peters, B. Batge, J. Brinckmann, D. P. Reinhardt, *J. Biol. Chem.* **2002**, *277*, 50795.
- [18] P. L. Zeeuwen, I. M. van Vlijmen-Willems, B. J. Jansen, G. Sotiropoulou, J. H. Curfs, J. F. Meis, J. J. Janssen, R. F. van Ruissen, J. Schalkwijk, *J. Invest. Dermatol.* **2001**, *116*, 693.
- [19] W. F. Daamen, S. T. Nillesen, T. Hafmans, J. H. Veerkamp, M. J. van Luyn, T. H. van Kuppevelt, *Biomaterials* **2005**, *26*, 81.
- [20] G. Lammers, C. Gilissen, S. T. Nillesen, P. J. Uijtdewilligen, R. G. Wismans, J. A. Veltman, W. F. Daamen, T. H. van Kuppevelt, *Biomaterials* **2010**, *31*, 8299.
- [21] R. A. Irizarry, B. Hobbs, F. Collin, Y. D. Beazer-Barclay, K. J. Antonellis, U. Scherf, T. P. Speed, *Biostatistics* **2003**, *4*, 249.
- [22] E. S. Lander, L. M. Linton, B. Birren, C. Nusbaum, M. C. Zody, J. Baldwin, K. Devon, K. Dewar, M. Doyle, W. FitzHugh, R. Funke, D. Gage, K. Harris, A. Heaford, J. Howland, L. Kann, J. Lehoczy, R. LeVine, P. McEwan, K. McKernan, J. Meldrum, J. P. Mesirov, C. Miranda, W. Morris, J. Naylor, C. Raymond, M. Rosetti, R. Santos, A. Sheridan, C. Sougnez, N. Stange-Thomann, N. Stojanovic, A. Subramanian, D. Wyman, J. Rogers, J. Sulston, R. Ainscough, S. Beck, D. Bentley, J. Burton, C. Clee, N. Carter, A. Coulson, R. Deadman, P. Deloukas, A. Dunham, I. Dunham, R. Durbin, L. French, D. Grafham, S. Gregory, T. Hubbard, S. Humphray, A. Hunt, M. Jones, C. Lloyd, A. McMurray, L. Matthews, S. Mercer, S. Milne, J. C. Mullikin, A. Mungall, R. Plumb, M. Ross, R. Shownkeen, S. Sims, R. H. Waterston, R. K. Wilson, L. W. Hillier, J. D. McPherson, M. A. Marra, E. R. Mardis, L. A. Fulton, A. T. Chinwalla, K. H. Pepin, W. R. Gish, S. L. Chissoe, M. C. Wendl, K. D. Delehaunty, T. L. Miner, A. Delehaunty, J. B. Kramer, L. L. Cook, R. S. Fulton, D. L. Johnson, P. J. Minx, S. W. Clifton, T. Hawkins, E. Branscomb, P. Predki, P. Richardson, S. Wenning, T. Slezak, N. Doggett, J. F. Cheng, A. Olsen, S. Lucas, C. Elkin, E. Uberbacher, M. Frazier, R. A. Gibbs, D. M. Muzny, S. E. Scherer, J. B. Bouck, E. J. Sodergren, K. C. Worley, C. M. Rives, J. H. Gorrell, M. L. Metzker, S. L. Naylor, R. S. Kucherlapati, D. L. Nelson, G. M. Weinstock, Y. Sakaki, A. Fujiyama, M. Hattori, T. Yada, A. Toyoda, T. Itoh, C. Kawagoe, H. Watanabe, Y. Totoki, T. Taylor, J. Weissbach, R. Heilig, W. Saurin, F. Artiguenave, P. Brottier, T. Bruls, E. Pelletier, C. Robert, P. Wincker, D. R. Smith, L. Doucette-Stamm, M. Rubenfield, K. Weinstock, H. M. Lee, J. Dubois, A. Rosenthal, M. Platzer, G. Nyakatura, S. Taudien, A. Rump, H. Yang, J. Yu, J. Wang, G. Huang, J. Gu, L. Hood, L. Rowen, A. Madan, S. Qin, R. W. Davis, N. A. Federspiel, A. P. Abola, M. J. Proctor, R. M. Myers, J. Schmutz, M. Dickson, J. Grimwood, D. R. Cox, M. V. Olson, R. Kaul, C. Raymond, N. Shimizu, K. Kawasaki, S. Minoshima, G. A. Evans, M. Athanasiou, R. Schultz, B. A. Roe, F. Chen, H. Pan, J. Ramser, H. Lehrach, R. Reinhardt, W. R. McCombie, B. M. de la, N. Dedhia, H. Blocker, K. Hornischer, G. Nordsiek, R. Agarwala, L. Aravind, J. A. Bailey, A. Bateman, S. Batzoglou, E. Birney, P. Bork, D. G. Brown, C. B. Burge, L. Cerutti, H. C. Chen, D. Church, M. Clamp, R. R. Copley, T. Doerks, S. R. Eddy, E. E. Eichler, T. S. Furey, J. Galagan, J. G. Gilbert, C. Harmon, Y. Hayashizaki, D. Haussler, H. Hermjakob, K. Hokamp, W. Jang, L. S. Johnson, T. A. Jones, S. Kasif, A. Kasprzyk, S. Kennedy, W. J. Kent, P. Kitts, E. V. Koonin, I. Korf, D. Kulp, D. Lancet, T. M. Lowe, A. McLysaght, T. Mikkelsen, J. V. Moran, N. Mulder, V. J. Pollara, C. P. Ponting, G. Schuler, J. Schultz, G. Slater, A. F. Smit, E. Stupka, J. Szustakowski,

- D. Thierry-Mieg, J. Thierry-Mieg, L. Wagner, J. Wallis, R. Wheeler, A. Williams, Y. I. Wolf, K. H. Wolfe, S. P. Yang, R. F. Yeh, F. Collins, M. S. Guyer, J. Peterson, A. Felsenfeld, K. A. Wetterstrand, A. Patrinos, M. J. Morgan, J. P. de Jong, J. J. Catanese, K. Osoegawa, H. Shizuya, S. Choi, Y. J. Chen, *Nature* **2001**, *409*, 860.
- [23] J. G. Bergboer, G. S. Tjabringa, M. Kamsteeg, I. M. van Vlijmen-Willems, D. Rodijk-Olthuis, P. A. Jansen, J. Y. Thuret, M. Narita, A. Ishida-Yamamoto, P. L. Zeeuwen, J. Schalkwijk, *Am. J. Pathol.* **2011**, *178*, 1470.
- [24] T. Cheng, G. S. Tjabringa, I. M. van Vlijmen-Willems, K. Hitomi, P. E. van Erp, J. Schalkwijk, P. L. Zeeuwen, *Br. J. Dermatol.* **2009**, *161*, 253.
- [25] G. J. de Jongh, P. L. Zeeuwen, M. Kucharekova, R. Pfundt, P. G. van der Valk, W. Blokk, A. Dogan, P. S. Hiemstra, P. C. van de Kerkhof, J. Schalkwijk, *J. Invest. Dermatol.* **2005**, *125*, 1163.
- [26] R. M. Gallucci, D. K. Sloan, J. M. Heck, A. R. Murray, S. J. O'Dell, *J. Invest. Dermatol.* **2004**, *122*, 764.
- [27] T. D. Schmittgen, K. J. Livak, *Nat. Protoc.* **2008**, *3*, 1101.
- [28] P. A. Jansen, M. Kamsteeg, D. Rodijk-Olthuis, I. M. van Vlijmen-Willems, G. J. de Jongh, M. Bergers, G. S. Tjabringa, P. L. Zeeuwen, J. Schalkwijk, *J. Invest. Dermatol.* **2009**, *129*, 2167.
- [29] K. Gosselin, E. Deruy, S. Martien, C. Vercamer, F. Bouali, T. Dujardin, C. Slomianny, L. Houel-Renault, F. Chelli, Y. De Launoit, C. Abbadie, *Am. J. Pathol.* **2009**, *174*, 423.
- [30] G. Lammers, G. S. Tjabringa, J. Schalkwijk, W. F. Daamen, T. H. Van Kuppevelt, *Biomaterials* **2009**, *30*, 6213.
- [31] S. L. Haynes, C. A. Shuttleworth, C. M. Kielty, *Br. J. Dermatol.* **1997**, *137*, 17.
- [32] E. J. O'Keefe, M. L. Chiu, R. E. Payne, Jr., *J. Invest. Dermatol.* **1988**, *90*, 767.
- [33] K. E. Rys-Sikora, R. L. Konger, J. W. Schoggins, R. Malaviya, A. P. Pentland, *Am. J. Physiol. Cell Physiol.* **2000**, *278*, C822.
- [34] J. Brinckmann, N. Hunzelmann, B. Kahle, J. Rohwedel, J. Kramer, M. A. Gibson, D. Hubmacher, D. P. Reinhardt, *Lab Invest.* **2010**, *90*, 739.
- [35] G. Cotta-Pereira, R. F. Guerra, S. Bittencourt-Sampaio, *J. Invest. Dermatol.* **1976**, *66*, 143.
- [36] R. G. Lopez, S. Garcia-Silva, S. J. Moore, O. Bereshchenko, A. B. Martinez-Cruz, O. Ermakova, E. Kurz, J. M. Paramio, C. Nerlov, *Nat. Cell Biol.* **2009**, *11*, 1181.
- [37] D. Scherer, R. Kumar, *Mutat. Res.* **2010**, *705*, 141.